Chemical Engineering Journal 446 (2022) 136984

Contents lists available at ScienceDirect

Chemical Engineering Journal

journal homepage: www.elsevier.com/locate/cej

Photocatalytic NO_x mitigation under relevant conditions using carbon nanotube-modified titania

Brian M. Everhart [a], Bailey McAuley [a], Ahmed Al Mayyahi [a], Bade Tonyali [b], Umut Yucel [b], Placidus B. Amama [a,*]

[a] Tim Taylor Department of Chemical Engineering, Kansas State University, Manhattan, KS 66506, USA

[b] Department of Animal Sciences and Industry, Food Science Institute, Kansas State University, Manhattan, KS 66506, USA

ARTICLE INFO

Keywords:
Photocatalysis
carbon nanotubes (CNTs)
TiO_2
NOx oxidation
DeNOx
Relative humidity

ABSTRACT

Although a majority of photocatalysts exhibit improved NO conversion to NO_2, the performance in the oxidation of NO_2, the more toxic form of NO_x, to nitrate remains a challenge; in addition, the performance of hybrid photocatalysts under practical conditions is unclear. This study demonstrates the use of carbon nanotube-TiO_2 (CNT-TiO_2) photocatalyst films for effective transformation of NO_x into nitrates. Using the objective figure of merit for NO_x abatement, $DeNO_x$ index, the catalyst performance in a laminar-flow reactor was evaluated under simulated conditions that are relevant in abating NO_x. The conditions probed include relative humidity (RH), initial NO_x concentration, reactor geometry (headspace distance), and state of the catalyst (fresh vs. recycled). Our results reveal CNT-TiO_2 significantly outperforms P25 despite exhibiting comparable NO conversion at low RH. P25 experiences a 66% reduction in DeNOx at high RH compared to low RH while CNT-TiO_2 only incurs a 27% reduction. For recycled photocatalysts, this disparity becomes even more pronounced; CNT-TiO_2 experiences a 49% reduction in DeNOx at high RH, whereas P25 experiences a 134% reduction. In addition, mass transfer from the bulk airflow limits NO conversion when the reactor headspace is too large (>3 mm), due to limited diffusion of NO_x to the photocatalyst surface. Our findings highlight the importance of headspace distance, a parameter that has mostly been overlooked in reactor design for photocatalytic oxidation of NO_x, but which dictates the optimal catalyst configuration for flue gas treatment. The remarkable $DeNO_x$ activity of CNT-TiO_2 over a wide range of RH levels is rationalized based on the ratio of physisorbed-to-chemisorbed water on the photocatalyst surface.

1. Introduction

Nitrogen oxides (NO_x), classified as criteria air pollutants by the Environmental Pollution Agency (EPA), are not only harmful at concentrations as low as 21 ppb (40ug/m^3) [1], but also react in atmosphere to generate tropospheric ozone, resulting in smog [2-4] and even contribute to particulate matter ($PM_{2.5}$) pollution concentrations via formation of nitrate aerosols [5]. NO_x is a generic term that refers to a mixture of nitrogen monoxide (NO) and dioxide (NO_2). Each of these pollutants is monitored by the EPA and World Health Organization (WHO) as they lead to respiratory issues including infection and irritation due to their ability to act as free radicals and induce high oxidative stress [6]. Over 90% of all atmospheric NO_x originates from anthropogenic sources, including energy production and distribution, and energy use in industry [4]. At combustion temperatures, the equilibrium constant for the following reaction increases exponentially, leading to substantial NO_x formation.

$$N_2 + O_2 \leftrightarrow 2NO \tag{1}$$

The conventional approach for reducing ambient NO_x concentrations requires elimination at the source via selective catalytic reduction (SCR) of flue gas or vehicle exhaust [7-10]. SCR introduces a reductant, such as ammonia or urea, to reduce NO_x to N_2, therefore reducing emissions at the source [9,10]. Because flue gas can contain hundreds of ppb of NO_x, even efficient conversion of NO_x by SCR results in emission with concentrations nearly 1000 × greater than the WHO permissible exposure limits [5,7]. Once NO_x disperses into the atmosphere, passive air purification techniques that are effective at sub-ppb level concentrations are required to convert the dilute NO_x concentrations to innocuous compounds.

* Corresponding author.
E-mail address: pamama@ksu.edu (P.B. Amama).

https://doi.org/10.1016/j.cej.2022.136984
Received 11 February 2022; Received in revised form 23 April 2022; Accepted 11 May 2022
Available online 13 May 2022

Heterogeneous photocatalysis using semiconductors is an effective method to eliminate atmospheric pollutants, including NO_x [11-27]. Photocatalytic oxidation of NO to nitrates first requires the generation of reactive oxygen species (ROS) via reactions with photogenerated excited electrons and holes (Equations 2–5). Once ROS are generated, NO oxidizes to NO_2 before converting to HNO_3 [28]:

$$TiO_2 + hv \rightarrow e^-_{CB} + h^+_{VB} \tag{2}$$

$$h^+_{VB} + H_2O_{ads} \rightarrow HO^{\cdot}_{ads} + H^+ \tag{3}$$

$$h^+_{VB} + HO^-_{ads} \rightarrow HO^{\cdot}_{ads} \tag{4}$$

$$e^-_{CB} + O_{2_{ads}} \rightarrow O^{\cdot -}_{2_{ads}} \tag{5}$$

The use of the gold standard TiO_2 (or P25) in photocatalysis suffers from two major limitations which severely limits its ability to efficiently remove atmospheric NO_x: rapid recombination rate of electrons and holes that diminish its efficiency, and a wide band gap ($E_g = 3.2$ eV for anatase) that confines its photoactivity to the UV range [19,29]. To address the former, studies have mostly focused on coupling with a noble metal/narrow band-gap semiconductor to form Schottky barriers or heterojunctions [13,30-32]. With the advent of nanocarbons, recent efforts have focused on exploiting their exceptional properties in designing efficient TiO_2-nanocarbon hybrid photocatalysts. Composites such as graphene-TiO_2 [19,21,29] and TiO_2-graphene-carbon nitride (g-C_3N_4) [21,33,34] have been used in photocatalytic oxidation of NO_x and have shown enhanced performance. While carbon nanotube-titania (CNT-TiO_2) photocatalysts have been applied in aqueous phase and gas phase studies involving other VOCs, there is surprisingly little research presented on their ability to degrade NO_x [35-37]. Liu et al., [35] investigated Cu-doped TiO_2 supported on CNTs for SO_2 and NO removal, but did not monitor NO_2 or NO_x concentrations. Li et al., [36] introduced CNTs to a traditional V_2O_5/TiO_2 catalyst for SCR of high NO concentrations (200 ppm) while Yen et al., [37] synthesized CNT-TiO_2 composites and tested their photocatalytic performance in 1000 ppb NO, obtaining modest conversion (32% NO_x conversion).

As shown in Equations (3) and (4), the generation of ROS requires adsorbed moisture. While a humid environment is favorable for generation of hydroxyl radicals due to increased adsorption of water molecules, elevated relative humidity can have an adverse effect on the conversion of NO_x. A few studies have shown the increase of NO conversion as humidity increases due to the increased generation of hydroxyl radicals [38,39]. Others, however, have reported humidity reduces NO conversion due to the competitive adsorption of water and the target pollutant molecule [14,40-44]. For oxidation of NO_x, there is therefore strong evidence that elevated humidity levels reduce NO_x conversion with traditional photocatalysts at low concentrations (<1ppb). This may be attributed in part to competitive adsorption of water and NO_x, where water molecules outnumber NO_x molecules by several orders of magnitude. On the other hand, high NO concentrations may benefit from elevated humidity, as a larger quantity of hydroxyl radicals would be required for oxidation reactions. While some of these studies concluded that NO conversion to NO_2 decreased with increasing humidity [14,41,44], others suggested that impaired NO_x oxidation is due to increased NO_2 generation despite relatively constant NO conversion [16,45]. Flue gas contains a large moisture concentration even when mixed with outdoor air. For successful coupling with existing remediation technology, it is important to understand the role of humidity in NO_x removal. Unfortunately, thus far, there is no conclusive understanding of the role of humidity in complete oxidation of NO_x to nitrates. In particular, there have been no reports on performance of CNT-TiO_2 photocatalysts at different humidity levels or their DeNO_x ability under any set of conditions.

In this study, CNT-TiO_2 hybrid photocatalyst films with optimum amount of CNTs were systematically investigated in NO_x oxidation under conditions that will enable their implementation as part of flue gas treatment system, downstream of SCR and prior to emission to the atmosphere. The desired photocatalyst is required to maintain effective De-NO_x ability under variable humidity, concentrations, catalyst conditions (fresh vs. used), and NO_x ratios. To determine the ability of a photocatalyst to eliminate the hazards associated with NO_x pollution, we have calculated the "De-NO_x index," a measure of photonic efficiency during NO_x abatement, for CNT-TiO_2 and a reference (P25) under the different oxidation conditions. Utilizing the De-NO_x index, an objective figure of merit for photocatalytic NO_x abatement, in tandem with relative NO_x oxidation has provided a better understanding of the photocatalyst performance. We have examined, for the first time, the effect of the reactor headspace distance thereby probing the role of mass transfer limitations in the photocatalytic process. Evaluation of the performance of recycled and fresh photocatalysts has provided valuable insight into their stability. Furthermore, the study provides valuable insight into the mechanism of NO_x oxidation, specifically as it pertains to NO_x storage selectivity and De-NO_x index using electron paramagnetic resonance spectroscopy (EPR) to determine the relative formation of hydroxyl and superoxide radicals for P25 and CNT-TiO_2 photocatalysts.

2. Experimental

2.1. Oxidation of CNTs

Multi-walled CNTs (MWCNTs) obtained from Times Nano (diameter 20–30 nm, purity > 95%) were photo-oxidized using H_2O_2 (Fisher Scientific, 30 wt%) via UV irradiation (White-Rodger Comfort plus UV200 2 Phillips TUV PL-L 60 W Bulbs) as described elsewhere [26,46]. In a typical batch, 1 g of CNTs were added to 400 mL of H_2O_2 in a round bottom flask. The mixture was sonicated for 15 min to uniformly disperse the CNTs. The CNTs were then heated to 60 °C under constant stirring and UV irradiation for 72 h; 50 mL of H_2O_2 was added every 24 h to make up for evaporation. The CNTs were vacuum filtered, rinsed with deionized water, and dried at 50 °C for 20 h to yield CNT powders with oxygen-containing functional groups on the surface.

2.2. Synthesis of CNT-TiO_2 hybrid photocatalyst

Synthesis of CNT-TiO_2 composite was performed via a modified sol–gel process, adapted from the method developed by Yu et al. [47]. The optimum amount of CNTs, as determined previously [26], was used in the synthesis of CNT-TiO_2 hybrids. First, functionalized CNTs were dispersed in ethanol for 30 min via sonication. Second, the titanium precursor, titanium (IV) isopropoxide (Sigma Aldrich, > 97%), was added dropwise to the ethanol/CNT solution and the resulting solution sonicated for 30 min to disperse the precursor. 80 mL nitric acid (0.001 M) was added to the solution to form a viscous, grey sol. The sols were sonicated for 30 min to ensure completion of the reaction before aging at 25 °C for 20 h. The product was vacuum filtered, rinsed with DI water and dried for 12 h at 80 °C. The resulting powders were crushed and calcined at 400 °C for 3 h. A total of 12 batches of photocatalyst were synthesized and were uniformly mixed into a large reserve to allow for use of identical fresh catalyst for each NO_x degradation experiment.

2.3. Coating of photocatalysts

The calcined CNT-TiO_2 photocatalysts were sieved to < 125 μm to increase powder uniformity and dispersion in solution. The photocatalyst powder was then dispersed in ethanol at a ratio of 0.15 g/ml and sonicated for 15 min following established steps by Weon and Choi [48]. The solution was drop cast onto glass slides (50 mm × 100 mm) via a pipet. A doctor blade set to a height of 250 μm above the slide was pulled across the surface to ensure a uniform coating thickness. Approximately 0.12 g of photocatalyst was deposited on each slide. The slides were then allowed to dry before being stored until testing.

2.4. Characterization of photocatalysts

X-ray diffraction (XRD) patterns of P-25 and the synthesized CNT-TiO_2 photocatalysts were obtained from a Rigaku MiniFlex II diffractometer utilizing a Cu Ka radiation source. Two-theta scanning angles from 10° to 80° degrees were taken with a step size of 0.02° and a scan speed of 2.0°/min. Scanning electron microscopy (SEM) with energy dispersive X-ray spectroscopy (EDX) was used to study the morphology and composition of photocatalysts. SEM images and EDX profiles were obtained using a Hitachi S5200, operated at 10 kV. The samples were characterized by UV–visible diffuse reflectance spectroscopy (UV–vis DRS) using a Shimadzu UV-2600 spectrometer with $BaSO_4$ as the background material. Photoluminescence (PL) spectroscopy was performed using a spectraMax i3x multi-mode microplate reader with an excitation wavelength of 360 nm. Thermogravimetric analysis (TGA) of photocatalysts was performed on a Shimadzu TGA-50 Analyzer. Roughly 8 mg of each sample was heated under a stream of air flow (10 mL/min) from room temperature to 600 °C at a rate of 5 °C/ min. X-ray photoelectron spectroscopy (XPS) data were collected using a PHI 5000 VersaProbe II (Physical Electronics Inc.) spectrometer with a monochromated Alk_α X-ray source, at ultrahigh vacuum ($1x10^{-9}$ bar) using an X-ray beam size of 100 µm. Survey spectra were recorded with pass energy (PE) of 117 eV, step size 1 eV and dwell time 20 ms, whereas high-energy resolution spectra were recorded with PE of 47 eV, step size 0.1 eV and dwell time 20 ms. Surface area and pore volume were derived from N_2 adsorption–desorption measurements at −196 °C. The BET method was applied to the adsorption isotherm (relative pressure range of 0.02–0.35) to calculate specific surface areas [49]. Pore-size distribution was obtained from the desorption isotherm at a relative pressure of 0.99 using the BJH model [50].

Electron paramagnetic resonance (EPR) spectroscopy measurements were performed using a stable nitroxide spin trap, 5,5-dimethyl-1-pyrroline-N-oxide (DMPO, Enzo Life Sciences, Plymouth Meeting, MI, USA) following the method described in Brezova et al., [51]. The catalysts (0.2 mg/mL) were dispersed in water with sodium dodecyl sulfate (SDS, 0.2 mg/mL) as a surfactant to inhibit catalyst particle aggregation in an ultrasonic bath for 15 min. Then, an aliquot of freshly-prepared DMPO solution (0.2 M) was added into the catalyst solution (10 mM DMPO final concentration), which was immediately irradiated with UV light under continuous stirring. After 5 min, an aliquot of solution (100 µL) was transferred to a borosilicate capillary tube, and sealed with vinyl plastic putty (Leica Microsystems, Wetzlar, Germany). The samples were inserted to the center of EPR cavity (SpinscanX, ADANI, Minsk, Belarus) analyzed using the following parameters: microwave frequency 93 kHz, microwave power 10 mW, center field 336.4 mT, sweep width 10 mT, and modulation amplitude 200 uT. The formation of DMPO-ROS spin adducts was quantified by calculating the total area under the curve via double-integration of the characteristic EPR peaks using GRAMS/AI™ Spectroscopy Software (Thermo Scientific™, Version 9).

The formation of superoxide radicals was investigated as follows. The photocatalysts were dispersed in water (10 mL) containing ethanol (1%, v/v) to final concentrations of 0.2 mg/mL and 1 mg/mL for P25 and CNT-TiO_2, respectively, using an ultrasonic bath for 15 min. An aliquot of freshly prepared DMPO solution (0.2 M) was added into the photocatalyst solution (50 mM final DMPO concentration), which was immediately irradiated with UV light under continuous stirring. After 5 min, 100 µL of solution was transferred to a capillary tube, and sealed with vinyl plastic putty. The samples were immediately inserted to the center of EPR cavity and analyzed using the parameters described above. In EPR experiments, dispersion of the catalyst in solution is imperative for accurate analysis of a catalyst's ability to generate hydroxyl radicals upon illumination. EPR experiments revealed the importance of catalyst dispersion for determining accurate OH radical generation.

2.5. Photocatalytic performance evaluation

Photocatalytic oxidation experiments were conducted at room temperature in a laminar-flow reactor constructed in accordance to ISO standards [52]. Two gas lines were connected to the reactor: the first contained 100 ppm NO in nitrogen while the second contained breathable air. Gases flowed through their respective mass flow controllers into a bubbler/bypass apparatus, enabling both humidity control and improved mixing of the gases upstream of the reactor. The relative humidity was monitored using a SensorPush HT1 humidity sensor. The reactor chamber was constructed from steel with a quartz glass window enabling UV light penetration to the photocatalyst surface. The sample holder within the reactor, constructed from PLA (polylactic acid polymer), held photocatalyst samples directly underneath the lighting apparatus. Photocatalysts were illuminated with four UVA/UVB Agro-Max Pure UV fluorescent lights (2 ft F24T5HO Pure UV, 75% UV-B / 25% UV-A) producing a UVA/UVB intensity reading of approximately 2 mW/cm^2. A Chemiluminescent 42C Low Source analyzer from Thermo Fisher Scientific was used to continuously measure the concentration of NO and NO_x. Fig. 1 a and b provide a schematic illustration of the reactor apparatus.

Prior to conducting each experiment, a different catalyst substrate was inserted into the sample holder and irradiated with UV light for ≥ 1 h with continuous airflow to remove any adsorbed contaminants. The lights were then turned off and NO_x was flowed with the air for 30 min to allow for adequate adsorption onto the photocatalyst surface. The UV lights were then turned on for 2 h under a constant flow of NO_x before the lights were turned off and NO_x levels allowed to re-equilibrate. Once each photocatalytic oxidation experiment was completed, concentrations of NO, NO_2, and NO_x were saved at one-minute intervals. Relative concentrations were determined by dividing the concentration at time t (C_t) by initial values (C_0). Average conversion percentages were determined after replicating each experiment (2–4 experiments per datum point). De-NO_x index values were calculated from these averaged relative concentration values.

Fig. 1c provides a graphic of the experimental conditions investigated. The effect of humidity was determined before investigating other conditions. Experiments were performed at 1000 ppb initial NO_x concentration and a total airflow of 3000 sccm at different RH levels (10–70% RH). Next, experiments were performed at different initial concentration levels (100–1000 ppb NO_x) at low (10% RH) and high (50% RH) humidity. After these experiments, the effect of headspace on the photocatalytic process (or the possibility of mass transfer limitations convoluting the DeNO_x index) was explored. These experiments were performed by changing the height of the sample holder (headspace distance), which involved directly changing the headspace in the reactor between 2 and 8 mm.

3. Results and discussion

3.1. Characterization of photocatalysts

XRD was used to determine the crystal structure of the photocatalysts. Fig. 2 (a) shows XRD patterns of P25 and CNT-TiO_2 and their corresponding peak assignments. Patterns for each individual CNT-TiO_2 batch prior to mixing are presented in Figure S1a; they confirm the batch-to-batch uniformity of the synthesized CNT-TiO_2. Clear differences between CNT-TiO_2 and P25 can be gleaned from the XRD patterns. Table 1 provides crystallographic (XRD) and surface area (BET) data. First, CNT-TiO_2 predominantly contains anatase (78%) with the remaining fraction is comprised of brookite (1 2 1). As expected, P25 contains a notable fraction of the rutile (1 1 0) crystal phase (18%), while containing no brookite (1 2 1). The presence of anatase and rutile in P25, and anatase and brookite in CNT-TiO_2 was confirmed with Raman spectroscopy (Figure S1c).

Another apparent difference is crystal size, as the peak width of CNT-

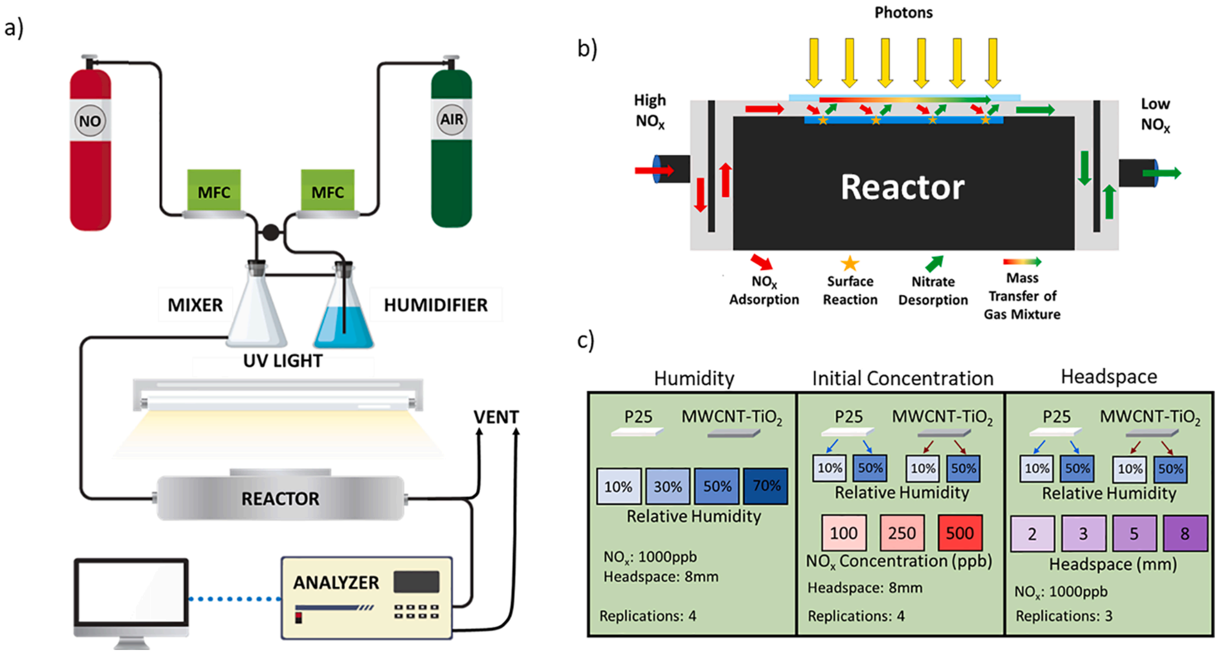

Fig. 1. (a) Schematic illustration of the photocatalytic reactor setup. (b) Schematic illustration of the laminar-flow reactor configuration constructed according to ISO standards showing NO_x flow and oxidation on photocatalyst surface. (c) Overview of experiments conducted.

TiO_2 is broader than that of P25. The crystallite size calculated from the Scherrer equation for CNT-TiO_2 and P25 is 8.1 nm and 21.4 nm, respectively. These results indicate a relatively smaller anatase crystal size in CNT-TiO_2 as compared to P25. The small anatase crystal size for the CNT-TiO_2 sample was in part due to the use of dilute (0.001 M) nitric acid during synthesis in place of deionized water. The use of nitric acid lowers the pH of the solution and has been shown to reduce crystallite size of TiO_2 powders [53]. Smaller crystallite size, along with the presence of CNTs, results in a higher surface area relative to P25. Figure S2 provides nitrogen adsorption–desorption isotherms, as well as optical microscopic images of catalyst films deposited on glass substrates. Tauc plots of the photocatalysts (inset of Fig. 2b) generated from their UV–vis spectra (Fig. 2b) were used to determine their band gaps assuming a direct allowed transition ($\gamma = 0.5$) and following the steps outlined in the literature [54]. The band gaps obtained for P25 and CNT-TiO_2 were $\sim$ 3.3 eV and $\sim$ 3.2 eV, respectively.

Fig. 2(c-e) shows SEM and EDS images of CNT-TiO_2 (c and d) and P25 (e and f). The images in panels (c) and (e) show the comparable macrostructure of both photocatalysts, and the small crystallite size of CNT-TiO_2 is verified by the SEM image of the microstructure (Figure S1). EDS results showing the elemental compositions are presented as insets in panels (d) and (f). P25 and CNT-TiO_2 contain 2.1 wt% and 4.2 wt% of carbon, respectively. We attribute the carbon present in P25 to background contamination; thus, the estimate of the actual carbon concentration in CNT-TiO_2 is approximately 2 wt%, slightly higher than the nominal concentration of 1 wt%. A carbon concentration of 2 wt% in CNT-TiO_2 may indicate the reduced yield of TiO_2 during the synthesis process. Additional characterization of the catalyst films are summarized in the supplementary section (Tables S1-S2).

3.2. *Effect of humidity*

Representative photocatalytic oxidation profiles in Fig. 3 show typical degradation of NO, NO_2 and NO_x on CNT-TiO_2 and P25 at low (10% RH) and high humidity (50% RH). Oxidation profiles in each figure has four distinct regions labelled 1– 4: (1) initiation of NO_x flow indicated by the steep rise in relative concentration ($\sim$10 min), (2) NO_x equilibration with the lights off ($\sim$30 min), (3) oxidation under illumination ($\sim$120 min), and (4) NO_x re-equilibration after lights are shut off ($\sim$160 min). When NO_x flow is initiated, a slightly higher concentration flows through the reactor to increase adsorption before the flow decreases to the desired concentration. At low RH (Fig. 3a-c), when the lights are turned on, profiles for NO, NO_2, and NO_x all immediately decrease to roughly half of the initial concentrations for both CNT-TiO_2 and P25. However, at 50% RH (Fig. 3d-f) the NO_2 degradation profiles for the photocatalysts show stark contrast in their relative concentrations, leading to notable differences in the overall NO_x profiles. While the NO_2 profile for the CNT-TiO_2 photocatalyst is substantially reduced in concentration under illumination, the NO_2 profile for P25 actually increases to values even higher than the initial concentration. Despite differences in the concentration profiles under illumination, concentrations of NO, NO_2, and NO_x, all quickly re-equilibrate back to a concentration of 1000 ppb after the lights are turned off before NO_x flow is shut off and the concentrations decrease sharply as air purges the system.

To further investigate the photocatalytic performance under different conditions, the DeNO_x index, an objective figure of merit for photocatalytic NO_x abatement, was used. The index provides a measurement of the overall photocatalyst performance in NO_x removal, as it considers NO conversion as well as NO storage selectivity, defined as the percentage of NO completely oxidized to nitrates versus the total amount of NO oxidized to NO_2. To calculate the DeNO_x index, the photonic efficiency for NO, NO_2, and NO_x must first be calculated using the following equation [17]:

$$\xi = \frac{(c_d - c_i)\dot{V}p}{\varphi ART} \tag{6}$$

where ξ represents the photonic efficiency of a given species; c_d and c_i the species concentrations in the dark and under illumination, respectively; $\dot{V}$ the volumetric flow rate; p the pressure in the system (1 atm for this work); and φ the photon flux at the photocatalyst surface, which is dependent on the wavelength of light (320 nm) and intensity (20 W/m^2). A, R, and T, are the catalyst irradiated area (5 cm $\times$ 10 cm), gas constant, and temperature (K), respectively. Once the photonic efficiency was calculated for each species, DeNO_x and NO_x storage selectivity (S) were calculated via the following equations:

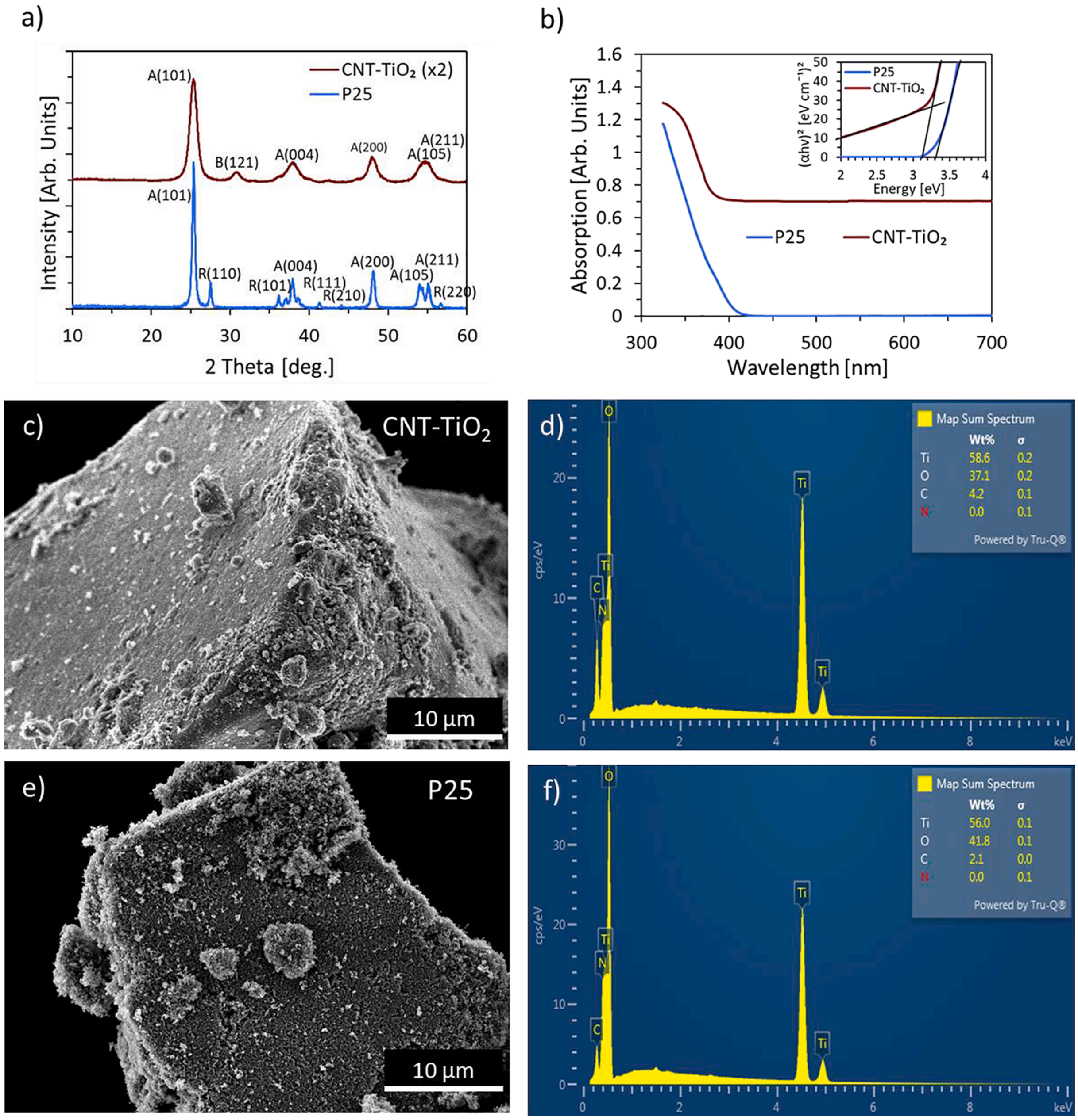

Fig. 2. (a) XRD patterns for CNT-TiO_2 (red) and P25 (blue) photocatalysts. (b) UV–Vis spectra of CNT-TiO_2 (red) and P25 (blue) photocatalysts (inset: Tauc plots of the photocatalysts). SEM images of CNT-TiO_2 (c) and P25 (e), and corresponding EDS spectra and chemical composition including weight percentage of carbon for CNT-TiO_2 (d) and P25 (f).

Table 1
Catalyst powder characterization.

	P25	CNT-TiO₂
Surface Area (m^2/g)[a]	51.6	131.0
Average Pore Diameter (nm)[a]	24.2	7.2
Total Pore Volume (cm^3/g)[a]	0.31	0.24
Anatase Content (wt%)[b]	81.9	77.8
Rutile Content (wt%)[b]	18.1	0.0
Brookite Content (wt%)[b]	0.0	22.2
Anatase Crystal Size (nm)[b]	21.4	8.1

[a] Nitrogen physisorption
[b] XRD

$$\xi_{DeNO_x} = \xi_{NO_x}\left(3 - \frac{2}{S}\right) \quad (7)$$

$$S = \frac{\xi_{NO_x}}{\xi_{NO}} \quad (8)$$

As discussed above, while the performance of the photocatalysts in NO oxidation are comparable irrespective of RH levels, there is a sharp contrast in performance in NO_2 conversion. Several studies [18,19,22,34,38,55] involving TiO_2 and TiO_2-based hybrids also show high performance in the conversion of NO_x to NO_2 under elevated humidity levels; however, their performance in the subsequent oxidation of NO_2 to nitrates that is critical in NO_x abatement is either low or not reported. Fig. 4a shows initial concentrations of NO and NO_2 at 1000 ppb total NO_x while Fig. 4b and c show reduction in relative concentration of NO, NO_2, and NO_x as a function of RH for P25 and CNT-TiO_2.

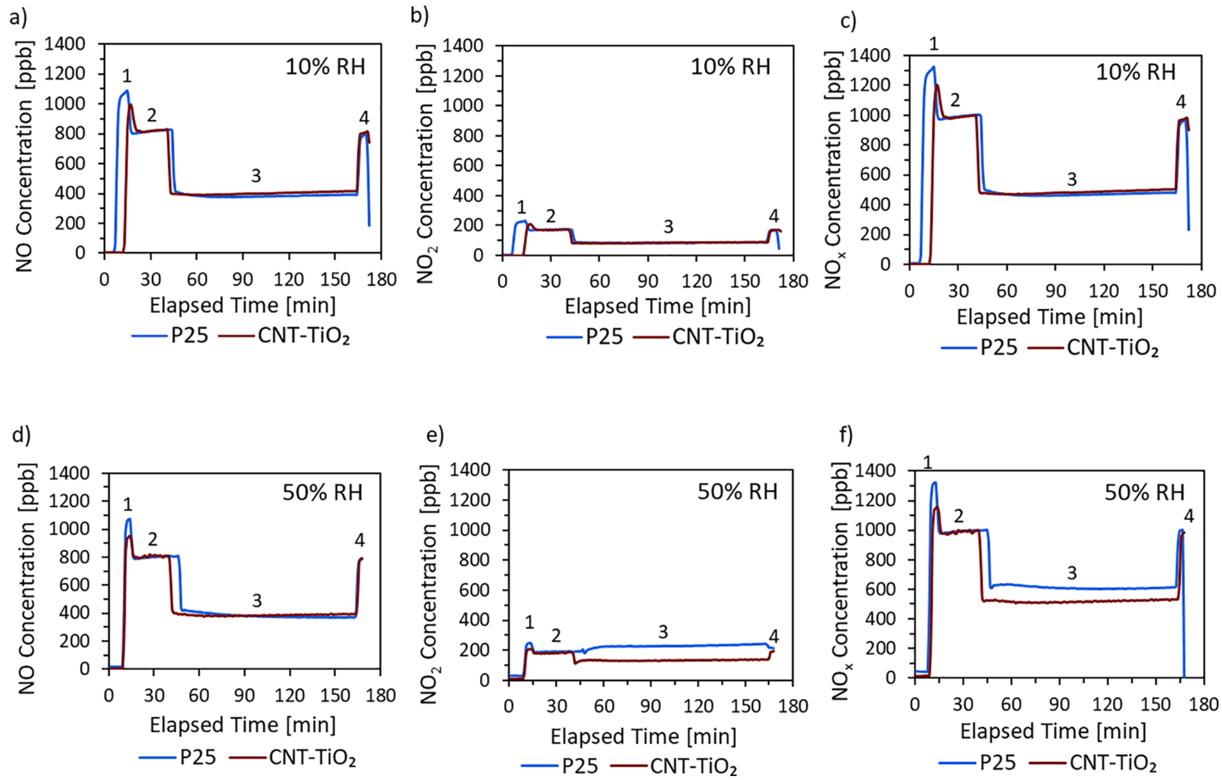

Fig. 3. Representative NOx degradation profiles at over 2 h using an initial NO_x concentration of 1000 ppb at low humidity (10% RH) for NO (a), NO_2 (b), and NO_x (c); and at high humidity (50% RH) for NO (d), NO_2 (e), NO_x (f). Each degradation profile has four distinct regions: (1) initiation of NO_x flow indicated by the steep rise in relative concentration (~10 min), (2) NO_x equilibration with the lights off (~30 min), (3) degradation under illumination (~120 min), and (4) NO_x re-equilibration after lights are shut off (~10 min).

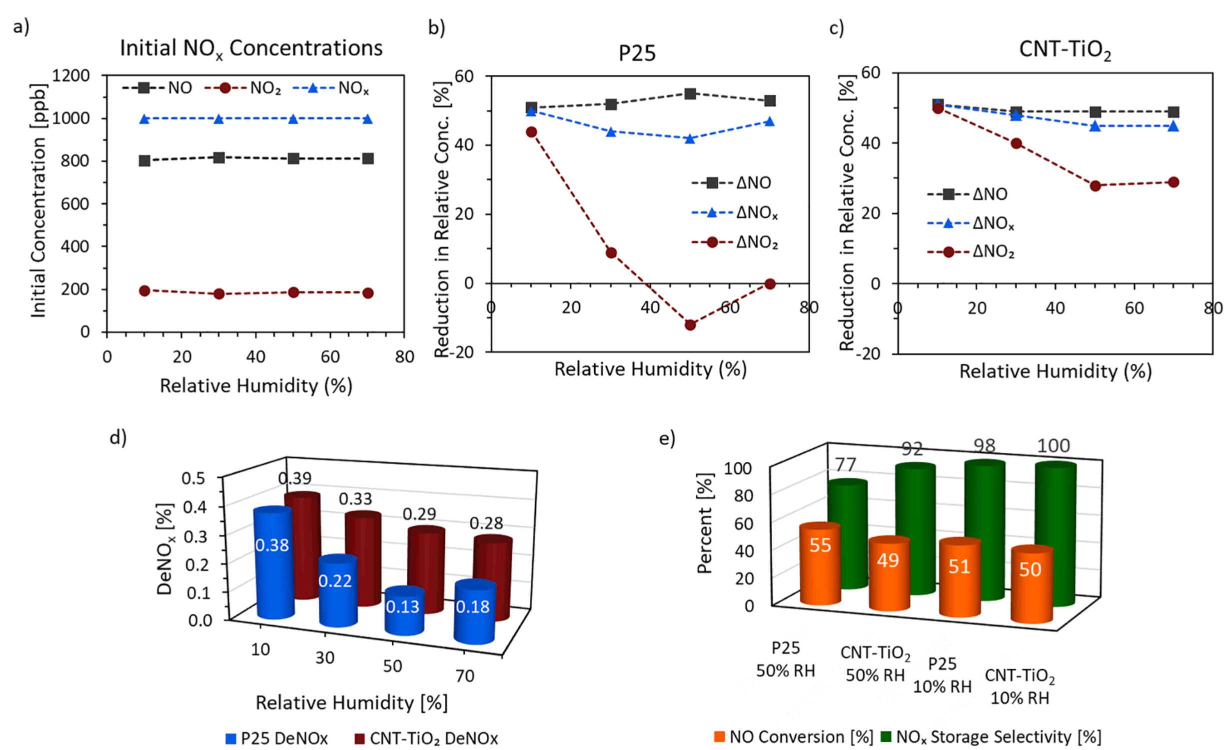

Fig. 4. Profiles of NO, NO_2, and NO_x concentrations as a function of RH: (a) initial NOx concentrations, (b) reduction in relative concentrations for P25, and (c) reduction in relative concentrations for CNT-TiO_2. (d) $DeNO_x$ index for P25 and CNT-TiO_2 as a function of RH. (e) NO conversion and NO_x storage selectivity at low and high RH for each catalyst. Experiments were performed at 1000 ppb initial NO_x concentration.

The reduction in relative concentration for NO (ΔNO), NO_2 (ΔNO_2) and NO_x (ΔNO_x) were calculated according to the following equations:

$$\Delta NO = (NO_{in} - NO_{out})/NO_{in} \quad (9)$$

$$\Delta NO_2 = (NO_{2in} - NO_{2out})/NO_{2in} \quad (10)$$

$$\Delta NO_x = (NO_{xin} - NO_{xout})/NO_{xin} \quad (11)$$

The relative NO, NO_2, and NO_x degradation percentages are shown for NO, NO_2, and NO_x in Table S3. The calculated $DeNO_x$ values at different RH levels are shown in Fig. 4d, while Fig. 4e shows NO conversion and NO_x storage selectivity. Clearly, at low RH levels, P25 and CNT-TiO_2 photocatalysts exhibit comparable $DeNO_x$ and selectivity, whereas at elevated RH levels, CNT-TiO_2 significantly outperforms P25 in terms of $DeNO_x$ despite comparable NO conversion due to higher NO_2 selectivity. Fig. 4d clearly illustrates the inferior $DeNO_x$ index of P25 even at 30% RH and performs even worse at both 50% and 70% RH. Conversely, CNT-TiO_2 experiences only a small decrease in $DeNO_x$ at elevated humidity and maintains high NO_x storage selectivity. Therefore, CNT-TiO_2 outperforms P25 in terms of $DeNO_x$ despite converting slightly less NO overall.

$DeNO_x$ index is particularly important in evaluating the abatement of NO_x pollution, as conversion to nitrates is imperative, rather than partial

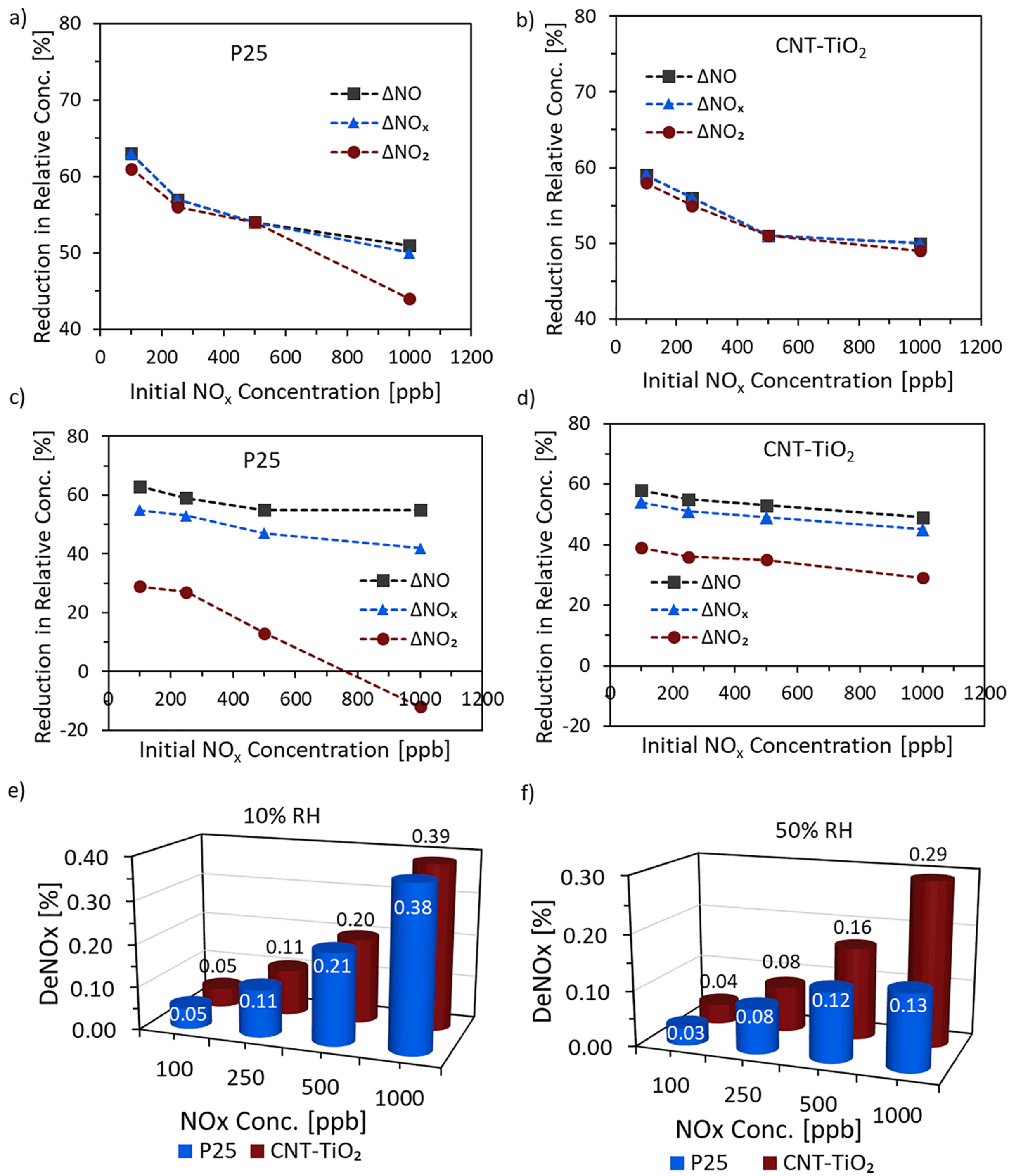

Fig. 5. Reduction in relative concentration profiles of NO, NO_2, and NO_x versus initial NO_x concentration at low RH (10%) for P25 (a) and CNT-TiO_2 (b) and high RH (50%) for P25 (c) and CNT-TiO_2 (d). (e) $DeNO_x$ index for P25 and CNT-TiO_2 as a function of initial concentration for 10% RH (e) and 50% RH (f).

conversion of NO to NO_2. Our extensive research on humidity levels around the world revealed few places experience humidity levels as low as 10% on a consistent basis [56]. Figure S3 provides humidity data of major cities, both in terms of relative humidity and absolute humidity (ppm). The humidity data indicate that realistic humidity conditions are at or above 50% RH, exceeding 5000 ppm water and reaching values as high as 15000 ppm or greater. Since air may be used as a diluent prior to the implementation of photocatalysis on treated flue gas waste streams, this necessitates the design of photocatalysts that exhibit high $DeNO_x$ index especially in humid environments.

3.3. Effect of initial concentration

The effect of initial concentration of NO_x on the oxidation of nitrogen oxides (NO, NO_2, and NO_x) and De-NO_x index for CNT-TiO_2 and P25 photocatalysts are shown in Fig. 5. The experiments were performed at low (10% RH) and high (50% RH) humidity levels. At low RH, the oxidation profiles of the different nitrogen oxides for P25 and CNT-TiO_2 are quite similar, especially at low initial concentrations (<500 ppb). However, at a NO_x concentration of 1000 ppb, it appears P25 starts to experience a decrease in NO_x storage selectivity, evidenced by the increase in the relative concentration of NO_2 compared to those of NO and NO_x. Corresponding plots of NO conversion and storage selectivity as functions of initial concentration can be found in Figure S4. These results show that NO conversion decreases with increasing initial concentration for both photocatalysts. Furthermore, P25 exhibits marginally higher NO conversion at all initial concentrations at low humidity; the trend becomes slightly more pronounced at high humidity. As observed in Fig. 5, even though CNT-TiO_2 exhibits a lower NO conversion, its $DeNO_x$ capability is superior especially at higher RH levels. CNT-TiO_2 shows a higher NO_x storage selectivity at all initial concentration at high humidity with the disparity becoming even more pronounced as initial concentration increases. The reduction in NO_2 conversion observed with P25 for an initial concentration of 1000 ppb (Fig. 5a) corresponds to a slight decrease in NO_x storage selectivity as shown in Figure S4a. Values of relative NO, NO_2, and NO_x degradation percentages for P25 and CNT-TiO_2 catalysts at different initial concentration for a) 50% and 10% RH from Fig. 5 are summarized in Table S4.

3.4. Effect of headspace

The effect of mass transfer in the reactor on NO_x oxidation is poorly understood even though it could be a competing factor in reactions carried out under different RH levels and initial NO_x concentrations. To test for mass transfer, experiments were performed at headspace distances of 8, 5, 3, and 2 mm, corresponding to residence times of 0.95, 0.59, 0.36, and 0.24 s, respectively (approximately 40–50% decrease in residence time at each interval). The effect of headspace on $DeNO_x$ for the photocatalysts is presented in Fig. 6a-b. The results reveal that mass transfer limitations significantly impact results at a headspace distance of 8 mm and even 5 mm, as NO conversion and $DeNO_x$ index values are comparable at 3 mm, despite a significantly lower residence time. If conversion stays constant as a function of residence time, then apparent reaction rate is much lower than the actual surface reaction rate. Mass

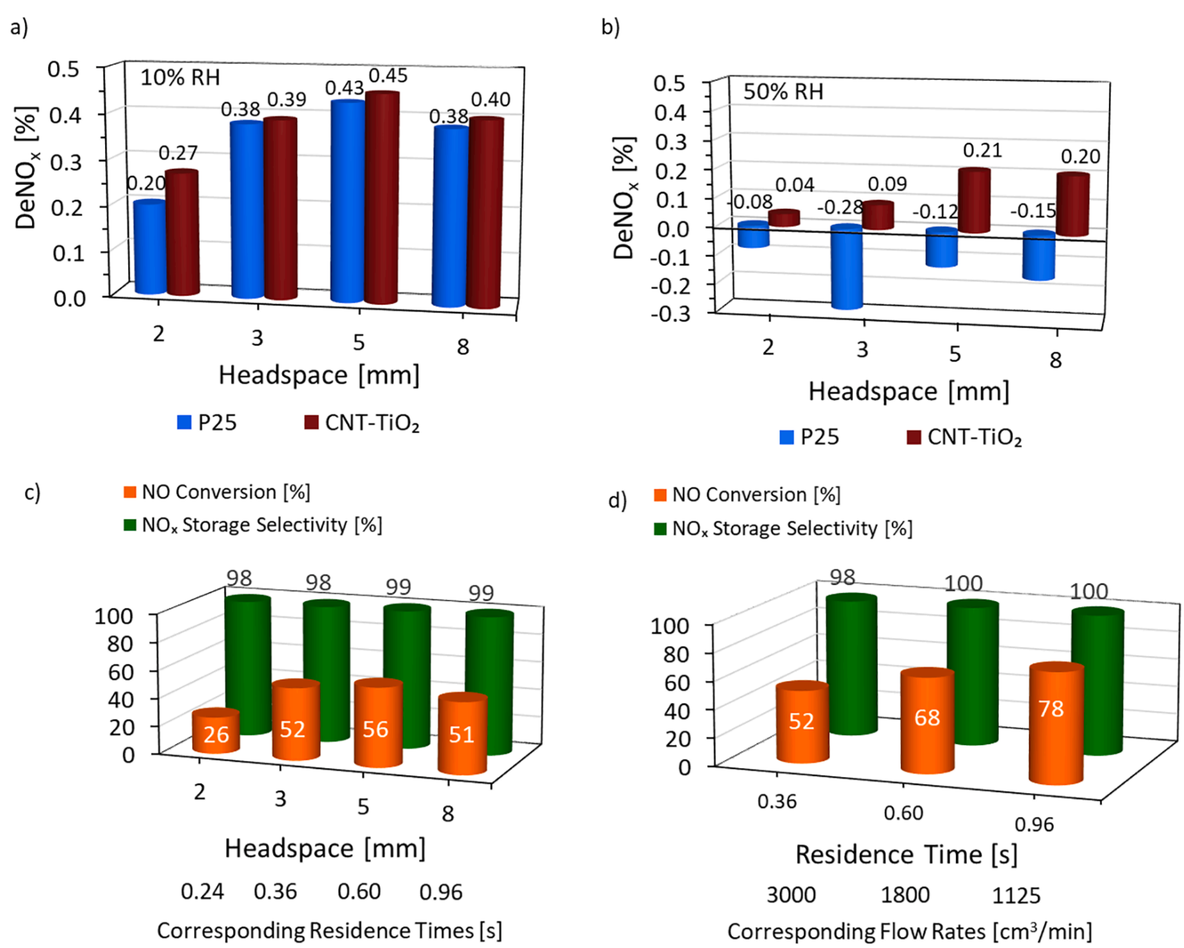

Fig. 6. $DeNO_x$ index for P25 and CNT-TiO_2 as a function of reactor headspace distance for low RH (10%) (a) and high RH (50%) (b). (c) NO conversion and NOx storage selectivity corresponding to (a). (d) NO conversion and NOx storage selectivity for photocatalytic reactions performed at different flow rates using a headspace distance of 3 mm at 10% RH. Flow rates in Figure (d) were chosen to equate residence times in Figure (c).

transfer from the bulk airflow therefore limits NO conversion when the reactor headspace is too large, due to limited diffusion of NO_x to the catalyst surface. To confirm these results, experiments were performed using P25 under low humidity at 3-mm headspace distance with different volumetric flowrates. Flowrate values were carefully selected to correspond to residence times used in the headspace experiments, allowing for comparison of NO conversion at identical residence times where mass transfer limitations were suspected. Fig. 6d shows NO conversion data obtained at 10% RH using a constant headspace distance (0.3 cm), but different volumetric flow rates; this is compared to results obtained at a constant volumetric flow rate, but different headspace distances (Fig. 6c). If no mass transfer limitations were present at headspace distances of 5 and 8 mm, NO conversion in Fig. 6c should correspond to the values obtained in Fig. 6d for residence times of 0.60 and 0.96 s. As expected, increasing residence time by decreasing flow rate while maintaining a constant headspace distance improved NO conversion. The conversions at residence times of 0.6 s and 0.96 s in Fig. 6d are significantly higher than their corresponding values in Fig. 6c at identical residence times, confirming the presence of mass transfer limitations at higher headspace values (>3 mm).

Under mass transfer limited conditions, transport of NO to the surface of the catalyst is limited, subsequently reducing the effective conversion rate of NO; this affects NO_2 generation and its conversion (or lack thereof) to nitrates. Furthermore, it allows extra time for the generated NO_2 to react with generated radicals, improving the apparent $DeNO_x$. Under conditions where mass transfer does not appear to be limiting, NO (based on NO conversion) may rapidly diffuse from the bulk flow and adsorbs on the catalyst surface, while NO_2 diffuses more rapidly from the boundary layer to the bulk flow, reducing the NO_x storage selectivity, and thus decreasing the $DeNO_x$ index. Our results highlight the importance of headspace distance, a parameter that has mostly been overlooked in photocatalytic reactor design and kinetic studies involving NO_x oxidation. It is therefore necessary to test photocatalytic reactors for mass transfer limitations to ensure NO conversion, selectivity, and $DeNO_x$ values are accurate.

3.5. Effect of photocatalyst stability and recycling

To probe the stability and reusability of the photocatalysts, we compared the performance of fresh and used photocatalysts after aging. Photocatalysts used in experiments to probe the effect of humidity (1000 ppb of NO_x, 10% and 50% RH) were aged for 12 months and the photocatalytic performance of the samples were reevaluated under similar conditions. As shown in Fig. 7, the humidity level has a significant impact on the performance of recycled catalysts. Both fresh and recycled P25 and CNT-TiO_2 show comparable performance at low humidity. At high humidity, however, P25 experiences substantially higher loss in catalytic performance than CNT-TiO_2. The reduced availability of active sites in P25 due to water adsorption at high humidity may be responsible for the poor activity. As discussed in Subsection 3.2, both photocatalysts experience a decrease in $DeNO_x$ at elevated humidity. P25 experiences a 66% reduction in $DeNO_x$ performance at high humidity compared to low humidity, but the CNT-TiO_2 catalyst only incurs a 27% reduction in $DeNO_x$ index. For recycled photocatalysts, this disparity becomes even more pronounced. CNT-TiO_2 experiences a 49% reduction in $DeNO_x$ at high humidity, whereas P25 experiences a 134% reduction. Several important observations can be made from Fig. 7. First, the recycled CNT-TiO_2 catalyst has better $DeNO_x$ ability than pristine P25. The result is especially important when considering photocatalytic oxidation of NO_x using atmospheric air where RH values are generally 50% or greater (Figure S3). Second, recycled P25 experiences a significantly higher drop-off in $DeNO_x$ at high RH (68% reduction) compared to recycled CNT-TiO_2 (22% reduction). It is apparent from these results that as P25 and CNT-TiO_2 photocatalysts are used over time, the disparity in their performance becomes even larger, confirming CNT-TiO_2 as a reusable and robust catalyst for NO_x oxidation.

3.6. Photocatalytic mechanism of NO_x oxidation

Clearly, humidity negatively impacts $DeNO_x$, even though NO conversion stays constant or increases with humidity. The change in $DeNO_x$ was the direct result of inhibited NO_x storage selectivity. As noted earlier, a number of studies have reported increasing NO_2 concentrations with humidity, particularly for TiO_2 photocatalysts [16,41,45]. Adsorbed water contributes to generation of hydroxyl radicals via Equations (3) and (4) while also occupying active sites, leading to counteracting phenomena during NO conversion. While reaction pathways for NO_x oxidation have been shown for both hydroxyl and oxygen radicals, most NO oxidation mechanisms focus on a multistep process dominated by hydroxyl radicals [28,57]. As shown in Equations 12–14, the process requires oxidation of NO to HONO, which reacts with a secondary hydroxyl radical, generating NO_2, before reacting with a tertiary hydroxyl radical to generate HNO_3. For catalysts exhibiting equal NO conversion, their different $DeNO_x$ index values could be attributed to incomplete oxidation of NO and increased generation of NO_2.

$$NO + HO^{\cdot} \rightarrow HONO \quad (12)$$

$$HONO + HO^{\cdot} \rightarrow NO_2 + H_2O \quad (13)$$

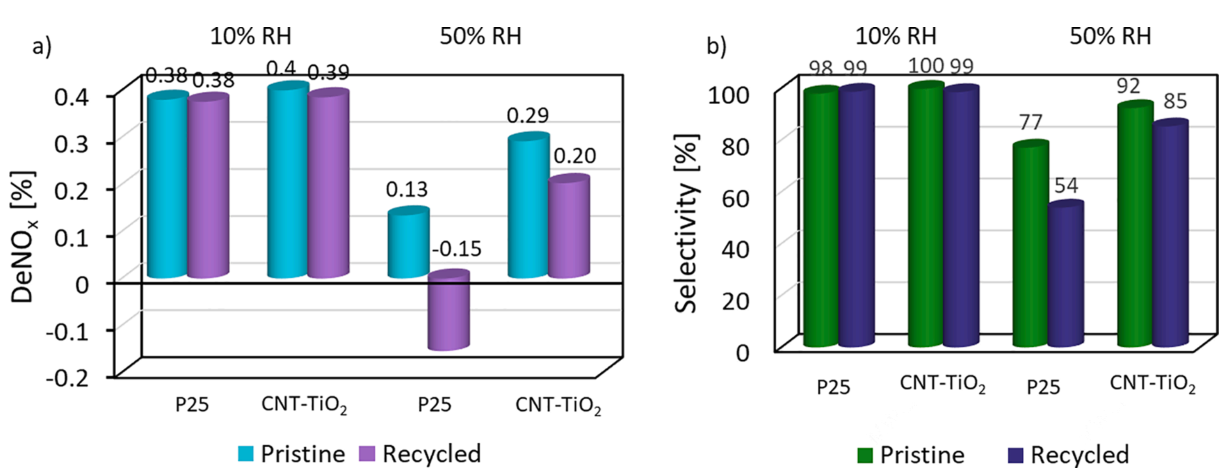

Fig. 7. (a) $DeNO_x$ index for pristine and recycled P25 and CNT-TiO_2 catalysts at 10% RH and 50% RH levels. (b) NO_x storage selectivity for pristine and recycled P25 and CNT-TiO_2 catalysts at 10% RH and 50% RH levels.

$$NO_2 + HO^{\cdot} \rightarrow HNO_3 \quad (14)$$

While this conventional mechanism relies on OH radicals involved in a multistep oxidation of NO to nitrates, some studies have suggested that hydroxyl radicals are not the dominant mechanism for NO_x oxidation [44,58,59]. In this case, superoxide radicals ($O_2^{\cdot-}$), generated from the reaction of adsorbed oxygen with the excited electron (Equation (5)), serve as a prominent reaction pathway for NO. Miyawaki et al., [16] also noted that NO_2 appeared to desorb more readily in a humid environment. These observations suggest the overall mechanism for NO_x oxidation to nitrates is more complicated than many of the current mechanisms suggest.

While no research has been reported on the effect of humidity on $DeNO_x$ using photocatalyst composites containing CNTs, a few studies have demonstrated that C_3N_4/TiO_2 photocatalysts can improve $DeNO_x$ in humid environments [20,23,33]. Generally, these composites improve the NO_x storage selectivity, leading to increased conversion of NO_2. Multiple studies [60-65] have highlighted the significant role of superoxide radicals, generated from reaction with the excited electron in the conduction band, in the photocatalytic oxidation of other pollutants. There is compelling evidence from the above studies that the incorporation of graphitic carbon nanomaterials in photocatalysts can increase the dominance of the oxidation pathway involving superoxide radicals relative to that with hydroxyl radicals. Furthermore, Furman et al., [66] demonstrated that water–solid matrices actually increase the stability and reactivity of superoxide radicals, while Aristidou et al., [67] suggested that superoxide radicals are more reactive on perovskite solar cells in the presence of physisorbed water in a humid environment.

To rationalize the stark difference in photocatalytic performance between P25 and CNT-TiO_2 under the different conditions and provide a deeper understanding into the oxidation mechanism, the photocatalyst

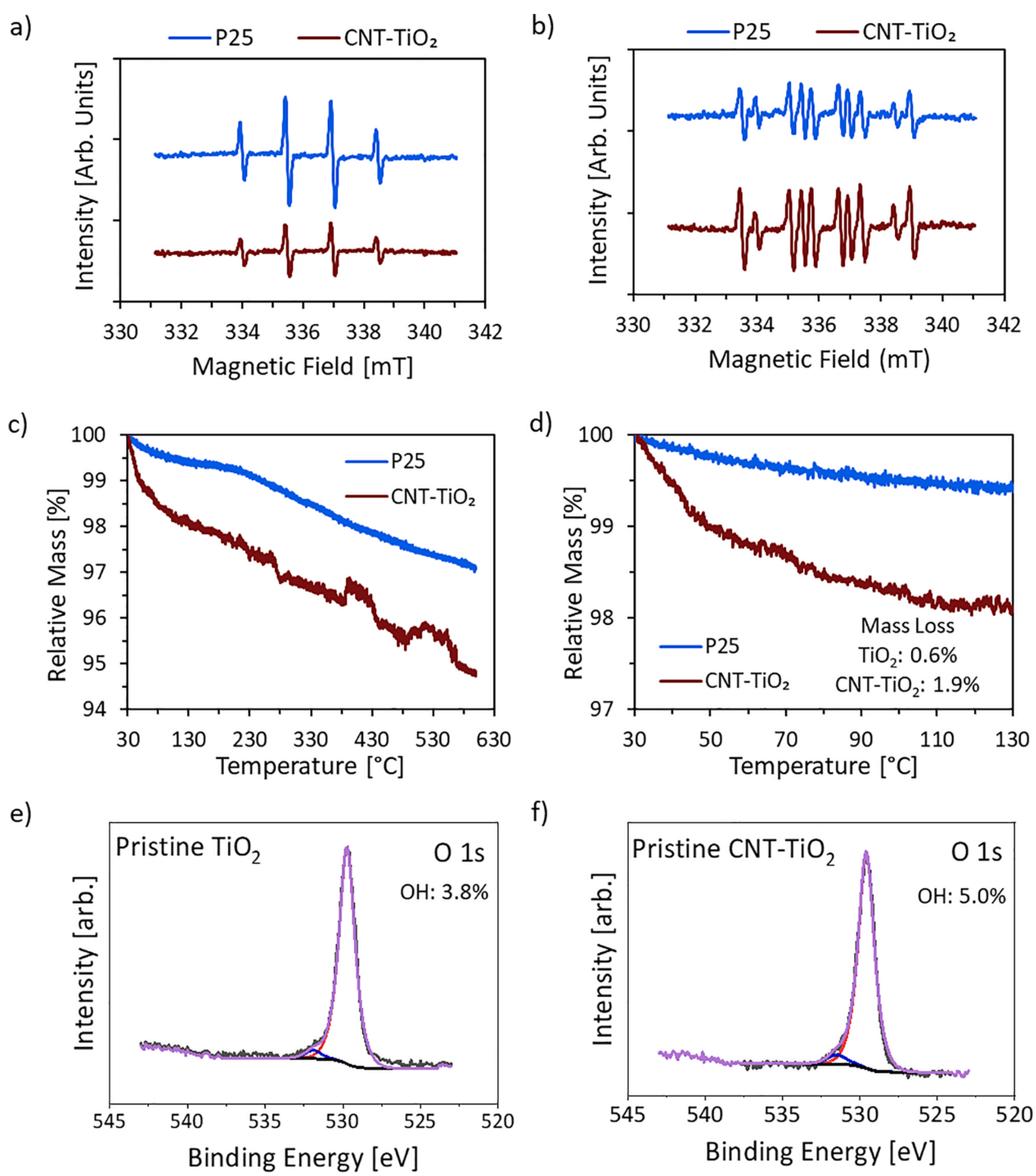

Fig. 8. (a-b) EPR spectra of DMPO-hydroxyl radical spin adducts produced from P25 and CNT-TiO_2 catalysts in (a) aqueous dispersion (0.2 mg/mL) and (b) water containing ethanol (1%, v/v, 0.2 mg/mL) after 5 min of UV irradiation. (c) TGA profiles of P25 and CNT-TiO_2 catalysts obtained using a ramp rate of 5 °C /min under air flow; (d) zoom-in version of (c) showing the temperature range of interest associated with desorption of physisorbed water. High-resolution XPS O 1 s spectra of P25 (e) and CNT-TiO_2 (f) catalysts.

activity was further investigated using other analyses (Fig. 8). EPR data in Fig. 8a-b provides semi-quantitative insight into hydroxyl and superoxide radical concentrations generated from P25 and CNT-TiO_2. The spin-trapped hydroxyl radical (DMPO-OH) adduct presents as a quartet with an intensity ratio of 1:2:2:1 [68,69]. EPR results indicate the CNT-TIO_2 catalyst generates a lower hydroxyl radical concentration than P25, evidenced by the reduction of the signal intensity in the quartet (Fig. 8a). This is consistent with the NO_x degradation data whereby NO to NO_2 conversion is slightly lower for CNT-TiO_2 than for P25. Despite the slightly lower generation of hydroxyl radicals, CNT-TiO_2 exhibits substantially higher NO_2 conversion particularly in a humid environment, highlighting the complex nature of the reaction.

In an aqueous environment, singlet oxygen reacts with DMPO to produce DMPO-O_2^-, which immediately decomposes to hydroxyl radical adducts [51,70]. Signal intensity in an aqueous environment is therefore correlated to formation of superoxide radicals; however, they are not observed directly because of their fast decomposition. EPR signals of superoxide radicals generated in presence of ethanol are shown in Fig. 8b. The complex EPR spectra was formed by the signal of hydroxyl radicals (same peak location as in Fig. 8a) and the larger peak signal of superoxide radicals next to the hydroxyl radicals. A similar EPR spectrum of DMPO-superoxide adducts was shown by Jackson et al., [71]. This semi-quantitative analysis proposed that the signal intensity ratio of superoxide radicals to hydroxyl radicals is higher in CNT-TIO_2 than in P25, indicating that the CNT-TiO_2 photocatalyst can generate more superoxide radicals than P25.

Furthermore, TGA data in Fig. 8c shows significant disparity in the mass loss experienced by the photocatalysts, particularly at low temperatures (<130 °C). For emphasis, the temperature range in Fig. 9c where physisorption occurs is shown in Fig. 8d. The greater mass loss experienced by CNT-TiO_2 suggests the presence of high amounts of physisorbed water compared to P25. However, analysis of the high-resolution XPS O 1 s peak (Fig. 8e and 8f) reveals comparable OH fractions, indicating comparable amounts of chemisorbed water due to the absence of physisorbed water in the ultra-high-vacuum XPS analysis chamber. From the TGA and XPS data, it is clear the ratio of physisorbed-to-chemisorbed water is much higher on the surface of CNT-TiO_2 compared to P25. Yang et al., [72] demonstrated that improved $DeNO_x$ in humidity was directly correlated to this ratio of physisorbed-to-chemisorbed water. In agreement with our work, we observe significant improvement in $DeNO_x$ index for CNT-TiO_2 photocatalyst in humid environment due to improved NO_2 conversion. PL data (Figure S7) indicate that the CNT-TiO_2 photocatalyst has a significantly lower intensity, which may suggest slower charge recombination [73,74]. It is important to note, however, that the suppressed PL spectra could have other causes, such as increased non-radiative recombination [73].

We therefore hypothesize that the CNT-TiO_2 catalyst generates a greater amount of superoxide radicals, which experience increased stability and reactivity due to the presence of physisorbed water. The O_2^- radicals directly oxidize NO to NO_3^-, effectively bypassing the generation of NO_2.

$$NO + O_2^- \rightarrow NO_3^- \quad (15)$$

This reaction pathway would be present on the surface of P25 as well, but to a lesser extent as fewer superoxide radicals are generated; these radicals likely degrade more rapidly, partaking in limited oxidation of NO_x due to the significantly lower amount of physisorbed water. In contrast, P25 appears to rely more heavily on NO_x oxidation via hydroxyl radicals. A schematic representation of the role of CNTs in improving NO_2 conversion on CNT-TiO_2 surface in a humid environment is presented in Fig. 9. Owing to the lower amounts of $OH^·$ radicals generated by CNT-TiO_2, NO conversion is lower, particularly in a humid environment. NO_x storage electivity on the CNT-TiO_2 catalyst is higher, however, because a greater amount of NO is directly oxidized to nitrates via O_2^- radicals. The increased reactivity of superoxide radicals may result from more efficient use of the radicals generated due to their

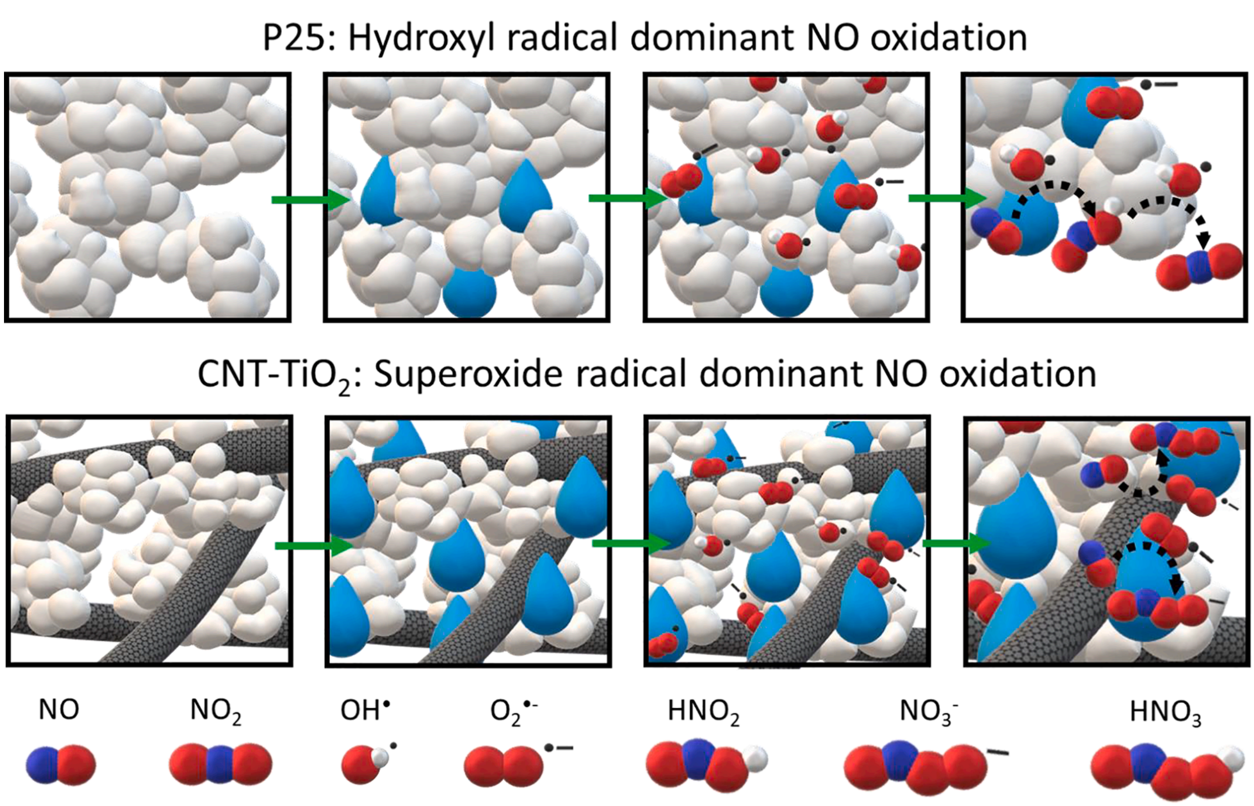

Fig. 9. Schematic illustration of the role of CNT in improving NO_2 conversion on CNT-TiO_2 in a humid environment. The relatively higher adsorbed water content on CNT-TiO_2 compared to the predominantly OH radical dominant oxidation of NO_x on P25 is hypothesized to increase stability and activity of superoxide radicals.

longer lifetimes and greater reactivity in the physisorbed water microenvironment. In this environment, it is also possible other ROS species, such as perhydroxyl radicals ($HO_2^{\cdot}$) and hydrogen peroxide (H_2O_2) may play a part in secondary reactions bypassing the traditional hydroxyl radical-assisted pathway.

The discussion of the mechanism would be incomplete without addressing the difference in surface area. We believe the effect of surface area is minor relative to the superoxide radical generation and reactivity discussed above. Yang et al., [72] demonstrated that two catalysts with very similar physisorbed-to-chemisorbed water ratios $\frac{H_2O}{OH+H_2O}$ had comparable NO, NO_2, and NO_x conversion efficiencies despite having significantly different surface areas (59.9 m^2/g vs. 321.1 m^2/g). We note that additional experiments with P25 indicated that there is a small effect of surface area on NO conversion, NO_x storage selectivity, and $DeNO_x$ when total catalyst weight is increased (Figure S8). However, since there are no significant differences in NO conversion or total catalyst weight (Table S2) for P25 and CNT-TiO_2, it is unlikely that surface area is playing a significant role in this case.

4. Conclusions

This work demonstrates the outstanding $DeNO_x$ and NO_x storage selectivity of CNT-TiO_2 photocatalysts under continuous flow under simulated conditions that will facilitate further removal of NOx from the waste stream of traditional flue gas treatment processes. While the CNT-TiO_2 catalyst significantly outperformed P25 at 50% RH and at higher initial NO_x concentrations (500 and 1000 ppb), the trend was less noticeable at initial concentrations of 250 ppb and 100 ppb. Headspace distance is an important factor in the evaluation of catalyst performance, as too large of a distance resulted in mass transfer limitations, preventing NO_x adsorption on the catalyst surface at a rate equivalent to the surface reaction. Further investigation of reactor headspace distance revealed that mass transfer limitations can convolute reaction results at a headspace distance>3 mm, despite having significantly longer residence times. These results highlight the need to test for mass transfer limitations in photocatalytic reactor with different configurations including those designed to ISO standards. Comparison of fresh and recycled photocatalysts revealed CNT-TiO_2 maintains performance at elevated humidity after long periods of shelf life, whereas P25 performance drops substantially from an already poor starting point. The significantly higher ratio of physisorbed-to-chemisorbed water on the surface of CNT-TiO_2 in comparison to P25 is used to rationalize the remarkable DeNOx performance observed with the former. This study offers a pathway for utilizing hybrid photocatalysts for efficient removal of NO_x downstream of industrial waste processing, to reduce the concentration of NO_x released to the atmosphere. The process has the potential of complementing current NO_x reduction technologies for flue gas and addressing industrial NO_x pollution at ground zero.

Declaration of Competing Interest

The authors declare that they have no known competing financial interests or personal relationships that could have appeared to influence the work reported in this paper.

Acknowledgments

This study was supported by the National Science Foundation under the NSF CAREER program (Grant No. 1653527). We are grateful to undergraduate students David Hawkins and David Ortiz for assisting with the catalytic testing.

Appendix A. Supplementary data

Supplementary data to this article can be found online at https://doi.org/10.1016/j.cej.2022.136984.

References

[1] M.J. Friedrich, Air pollution is greatest environmental threat to health, Global Health 319 (11) (2018) 1085.
[2] Y. Itano, H. Bandow, N. Takenaka, Y. Saitoh, A. Asayama, J. Fukuyama, Impact of NOx reduction on long-term ozone trends in an urban atmosphere, Sci. Total Environ. 379 (2007) 46–55.
[3] R. Atkinson, Atmospheric chemistry of VOCs and NOx, Atmos. Environ. 34 (2000) 2063–2101.
[4] Environmental Protection Agency, Nitrogen Oxides Emissions, in: U.S.E.P. Agency (Ed.) Report on the Environment, 2018.
[5] Ambient (outdoor) air pollution, World Health Organization, 2018.
[6] M. Kampa, E. Castanas, Human health effects of air pollution, Environ. Pollut. 151 (2) (2008) 362–367.
[7] X. Liu, H. Tan, Y. Wang, F. Yang, H. Mikulcic, M. Vujanovic, N. Duic, Low NOx combustion and SCR flow field optimization in a low volatile coal fired boiler, J Environ Manage 220 (2018) 30–35.
[8] R. Fuse, H. Kobayashi, Y. Ju, K. Maruta, T. Niioka, NOx emission from high-temperature air/methane counterflow diffusion flame, Int. J. Therm. Sci. 41 (2002) 693–698.
[9] F. Rezaei, A.A. Rownaghi, S. Monjezi, R.P. Lively, C.W. Jones, SOx/NOx removal from flue gas streams by solid adsorbents: A review of current challenges and future directions, Energy Fuels 29 (2015) 5467–5486.
[10] M. Koebel, M. Elsener, M. Kleemann, Urea-SCR: a promising technique to reduce NOx emissions from automotive diesel engines, Catal. Today 59 (2000) 335–345.
[11] J.S. Dalton, P.A. Janes, N.G. Jones, J.A. Nicholson, K.R. Hallam, G.C. Allen, Photocatalytic oxidation of NOx gases using TiO2: a surface spectroscopic approach, Environ. Pollut. 120 (2002) 415–422.
[12] S. Wang, H.M. Ang, M.O. Tade, Volatile organic compounds in indoor environment and photocatalytic oxidation: State of the art, Environ. Int. 33 (5) (2007) 694–705.
[13] K. Woan, G. Pyrgiotakis, W. Sigmund, Photocatalytic carbon-nanotube–TiO2 composites, Adv. Mater. 21 (2009) 2233–2239.
[14] T. Maggos, J.G. Bartzis, P. Leva, D. Kotzias, Application of photocatalytic technology for NOx removal, Appl. Phys. A 89 (2007) 81–84.
[15] S.-H. Yoon, S.-E. Oh, J.E. Yang, J.H. Lee, M. Lee, S. Yu, D. Pak, TiO2 Photocatalytic oxidation mechanism of As(III), Environ. Sci. Technol. 43 (2009) 864–869.
[16] J. Miyawaki, T. Shimohara, N. Shirahama, A. Yasutake, M. Yoshikawa, I. Mochida, S.-H. Yoon, Removal of NOx from air through cooperation of the TiO2 photocatalyst and urea on activated carbon fiber at room temperature, Appl. Catal. B 110 (2011) 273–278.
[17] J.Z. Bloh, A. Folli, D.E. Macphee, Photocatalytic NOx abatement: why the selectivity matters, RSC Adv. 4 (2014) 45726–45734.
[18] T. Giannakopoulou, N. Todorova, G. Romanos, T. Vaimakis, R. Dillert, D. Bahnemann, C. Trapalis, Composite hydroxyapatite/TiO2 materials for photocatalytic oxidation of NOx, Mater. Sci. Eng., B 177 (2012) 1046–1052.
[19] N.T.A. Trapalisa, T. Giannakopoulou, N. Boukos, T. Speliotis, D. Dimotikali, J. Yu, TiO2/graphene composite photocatalysts for NOx removal: A comparison of surfactant-stabilized graphene and reduced graphene oxide, Appl. Catal. B (2016) 634–647.
[20] I. Papailias, N. Todorova, T. Giannakopoulou, J. Yu, D. Dimotikali, C. Trapalis, Photocatalytic activity of modified g-C3N4/TiO2 nanocomposites for NOx removal, Catal. Today 280 (2017) 37–44.
[21] A. Nikokavoura, C. Trapalis, Graphene and g-C3N4 based photocatalysts for NOx removal: A review, Appl. Surf. Sci. 430 (2018) 18–52.
[22] D. Papoulis, K. Somalakidi, N. Todorova, C. Trapalis, D. Panagiotaras, D. Sygkridou, E. Stathatos, E. Gianni, A. Mavrikos, S. Komarneni, Sepiolite/TiO2 and metal ion modified sepiolite/TiO2 nanocomposites: synthesis, characterization and photocatalytic activity in abatement of NOx gases, Appl. Clay Sci. 179 (2019), 105156.
[23] M. Irfan, M. Sevim, Y. Koçak, M. Balci, Ö. Metin, E. Ozensoy, Enhanced photocatalytic NOx oxidation and storage under visible-light irradiation by anchoring Fe3O4 nanoparticles on mesoporous graphitic carbon nitride (mpg-C3N4), Appl. Catal. B 249 (2019) 126–137.
[24] P.B. Amama, K. Itoh, M. Murabayashi, Photocatalytic oxidation of trichloroethylene in humidified atmosphere, J. Mol. Catal. A: Chem. 176 (2001) 165–172.
[25] P.B. Amama, K. Itoh, M. Murabayashi, Gas-phase photocatalytic degradation of trichloroethylene on pretreated TiO2, Appl. Catal. B: Environ. 37 (2002) 321–330.
[26] B.M. Everhart, M. Baker-Fales, B. McAuley, E. Banning, H. Almkhelfe, T.C. Back, P. B. Amama, Hydrothermal synthesis of carbon nanotube–titania composites for enhanced photocatalytic performance, J. Mater. Res. 35 (2020) 1451–1460.
[27] A. Al Mayyahi, B.M. Everhart, T.B. Shrestha, T.C. Back, P.B. Amama, Enhanced charge separation in TiO2/nanocarbon hybrid photocatalysts through coupling with short carbon nanotubes, RSC, Advances 11 (2021) 11702–11713.
[28] J. Lasek, Y.-H. Yu, J.C.S. Wu, Removal of NOx by photocatalytic processes, J. Photochem. Photobiol., C 14 (2013) 29–52.
[29] M. Chen, Y. Huang, J. Yao, J.-J. Cao, Y. Liu, Visible-light-driven N-(BiO)2CO3/Graphene oxide composites with improved photocatalytic activity and selectivity for NOx removal, Appl. Surf. Sci. 430 (2018) 137–144.
[30] A. Zaleska, Doped-TiO2, a Review, Recent Patents on, Engineering (2008) 157–164.
[31] A.L. Linsebigler, G. Lu, J.T. Yates, Photocatalysis on TiO2 Surfaces: Principles, Mechanisms, and Selected Results, Chem. Rev. 95 (1995) 735–758.

[32] H. Chen, R. Yang, K. Zhu, W. Zhou, M. Jiang, Attenuating toluene mobility in loess soil modified with anion–cation surfactants, J. Hazardous Mater. 94 (2002) 191–201.
[33] T. Giannakopoulou, I. Papailias, N. Todorova, N. Boukos, Y. Liu, J. Yu, C. Trapalis, Tailoring the energy band gap and edges' potentials of g-C3N4/TiO2 composite photocatalysts for NOx Removal, Chem. Eng. J. 310 (2017) 571–580.
[34] Y.H.X. Song, M. Zheng, C. Wei, Solvent-free in situ synthesis of g-C3N4/{0 0 1} TiO2 composite with enhanced UV- and visible-light photocatalytic activity for NO oxidation, Appl. Catal. B (2016) 587–597.
[35] H. Liu, X. Yu, H. Yang, The integrated photocatalytic removal of SO2 and NO using Cu doped titanium dioxide supported by multi-walled carbon nanotubes, Chem. Eng. J. 243 (2014) 465–472.
[36] Q. Li, H. Yang, F. Qiu, X. Zhang, Promotional effects of carbon nanotubes on V2O5/TiO2 for NOX removal, J. Hazard. Mater. 192 (2011) 915–921.
[37] C.-Y. Yen, Y.-F. Lin, C.-H. Hung, Y.-H. Tseng, C.-C.-M. Ma, M.-C. Chang, H. Shao, The effects of synthesis procedures on the morphology and photocatalytic activity of multi-walled carbon nanotubes/TiO2nanocomposites, Nanotechnology 19 (2008), 045604.
[38] S. Devahasdin, C. Fan, K. Li, D.H. Chen, TiO2 photocatalytic oxidation of nitric oxide: transient behavior and reaction kinetics, J. Photochem. Photobiol., A 156 (1-3) (2003) 161–170.
[39] Q.L. Yu, H.J.H. Brouwers, Indoor air purification using heterogeneous photocatalytic oxidation, Part I: Experimental study, Applied Catalysis B: Environmental 92 (3-4) (2009) 454–461.
[40] G. Guo, Y. Hu, S. Jiang, C. Wei, Photocatalytic oxidation of NOx over TiO2/HZSM-5 catalysts in the presence of water vapor: Effect of hydrophobicity of zeolites, J. Hazard. Mater. 223–224 (2012) 39–45.
[41] L. Yang, A. Hakki, L. Zheng, M.R. Jones, F. Wang, D.E. Macphee, Photocatalytic concrete for NOx abatement: Supported TiO2 efficiencies and impacts, Cem. Concr. Res. 116 (2019) 57–64.
[42] X. Xie, C. Hao, Y. Huang, Z. Huang, Influence of TiO2-based photocatalytic coating road on traffic-related NOx pollutants in urban street canyon by CFD modeling, Sci. Total Environ. 724 (2020), 138059.
[43] G. Hüsken, M. Hunger, H.J.H. Brouwers, Experimental study of photocatalytic concrete products for air purification, Build. Environ. 44 (2009) 2463–2474.
[44] S. Laufs, G. Burgeth, W. Duttlinger, R. Kurtenbach, M. Maban, C. Thomas, P. Wiesen, J. Kleffmann, Conversion of nitrogen oxides on commercial photocatalytic dispersion paints, Atmos. Environ. 44 (2010) 2341–2349.
[45] C.H. Ao, S.C. Lee, Enhancement effect of TiO2 immobilized on activated carbon filter for the photodegradation of pollutants at typical indoor air level, Appl. Catal. B 44 (2003) 191–205.
[46] H. Almkhelfe, X. Li, P. Thapa, K.L. Hohn, P.B. Amama, Carbon nanotube-supported catalysts prepared by a modified photo-Fenton process for Fischer-Tropsch synthesis, J. Catal. 361 (2018) 278–289.
[47] Y. Yu, J.C. Yu, J.-G. Yu, Y.-C. Kwok, Y.-K. Che, J.-C. Zhao, L.u. Ding, W.-K. Ge, P.-K. Wong, Enhancement of photocatalytic activity of mesoporous TiO2 by using carbon nanotubes, Appl. Catal. A 289 (2) (2005) 186–196.
[48] S. Weon, W. Choi, TiO2 Nanotubes with Open Channels as Deactivation-Resistant Photocatalyst for the Degradation of Volatile Organic Compounds, Environ. Sci. Technol. 50 (2016) 2556–2563.
[49] S. Brunauer, P.H. Emmett, E. Teller, Adsorption of Gases in Multimolecular Layers, J. Am. Chem. Soc. 60 (1938) 309–319.
[50] E.P. Barrett, L.G. Joyner, P.P. Halenda, The Determination of Pore Volume and Area Distributions in Porous Substances. I. Computations from Nitrogen Isotherms, J. Am. Chem. Soc. 73 (1951) 373–380.
[51] V. Brezová, D. Dvoranová, A. Staško, Characterization of titanium dioxide photoactivity following the formation of radicals by EPR spectroscopy, Res. Chem. Intermed. 33 (2007) 251–268.
[52] I.O.f. Standardization, Fine ceramics (advanced ceramics, advanced technical ceramics) — Test method for air-purification performance of semiconducting photocatalytic materials —, Removal of nitric oxide, International Organization for Standardization, 2016.
[53] S. Mahshid, M. Askari, M.S. Ghamsari, Synthesis of TiO2 nanoparticles by hydrolysis and peptization of titanium isopropoxide solution, J. Mater. Process. Technol. 189 (2007) 296–300.
[54] K.A. Michalow, D. Logvinovich, A. Weidenkaff, M. Amberg, G. Fortunato, A. Heel, T. Graule, M. Rekas, Synthesis, characterization and electronic structure of nitrogen-doped TiO2 nanopowder, Catal. Today 144 (2009) 7–12.
[55] H. Wang, Z. Wu, W. Zhao, B. Guan, Photocatalytic oxidation of nitrogen oxides using TiO2 loading on woven glass fabric, Chemosphere 66 (2007) 185–190.
[56] Information (2021).
[57] V.-H. Nguyen, B.-S. Nguyen, C.-W. Huang, T.-T. Le, C.C. Nguyen, T.T. Nhi Le, D. Heo, Q.V. Ly, Q.T. Trinh, M. Shokouhimehr, C. Xia, S.S. Lam, D.-V. Vo, S.Y. Kim, Q.V. Le, Photocatalytic NOx abatement: Recent advances and emerging trends in the development of photocatalysts, J. Cleaner Prod. 270 (2020) 121912.
[58] T. Martinez, A. Bertron, E. Ringot, G. Escadeillas, Degradation of NO using photocatalytic coatings applied to different substrates, Build. Environ. 46 (2011) 1808–1816.
[59] K. Hashimoto, K. Wasada, N. Toukai, H. Kominami, Y. Kera, Photocatalytic oxidation of nitrogen monoxide over titanium(IV) oxide nanocrystals large size areas, J. Photochem. Photobiol., A 136 (2000) 103–109.
[60] J. Ryu, W. Choi, Effects of TiO2 Surface Modifications on Photocatalytic Oxidation of Arsenite: The Role of Superoxides, Environ. Sci. Technol. 38 (2004) 2928–2933.
[61] L. Cermenati, P. Pichat, C. Guillard, A. Albini, Probing the TiO2 Photocatalytic Mechanisms in Water Purification by Use of Quinoline, Photo-Fenton Generated OH· Radicals and Superoxide Dismutase, J. Phys. Chem. B 101 (14) (1997) 2650–2658.
[62] G.-H. Moon, D.-H. Kim, H.-i. Kim, A.D. Bokare, W. Choi, Platinum-like Behavior of Reduced Graphene Oxide as a Cocatalyst on TiO2 for the Efficient Photocatalytic Oxidation of Arsenite, Environ. Sci. Technol. Lett. 1 (2) (2014) 185–190.
[63] J.M. Monteagudo, A. Durán, M.R. Martínez, I. San Martín, Effect of reduced graphene oxide load into TiO2 P25 on the generation of reactive oxygen species in a solar photocatalytic reactor. Application to antipyrine degradation, Chem. Eng. J. 380 (2020) 122410.
[64] J. Zhong, H. Jiang, Z. Wang, Z. Yu, L. Wang, J.F. Mueller, J. Guo, Efficient photocatalytic destruction of recalcitrant micropollutants using graphitic carbon nitride under simulated sunlight irradiation, Environmental Science and Ecotechnology 5 (2021) 100079.
[65] N. Waiskopf, Y. Ben-Shahar, M. Galchenko, I. Carmel, G. Moshitzky, H. Soreq, U. Banin, Photocatalytic Reactive Oxygen Species Formation by Semiconductor-Metal Hybrid Nanoparticles, Toward Light-Induced Modulation of Biological Processes, Nano Letters 16 (7) (2016) 4266–4273.
[66] O. Furman, D.F. Laine, A. Blumenfeld, A.L. Teel, K. Shimizu, I.F. Cheng, R.J. Watts, Enhanced Reactivity of Superoxide in Water−Solid Matrices, Environ. Sci. Technol. 43 (5) (2009) 1528–1533.
[67] N. Aristidou, C. Eames, M.S. Islam, S.A. Haque, Insights into the increased degradation rate of CH3NH3PbI3 solar cells in combined water and O2 environments, J. Mater. Chem. A 5 (48) (2017) 25469–25475.
[68] M. Mrowetz, E. Selli, Enhanced photocatalytic formation of hydroxyl radicals on fluorinated TiO2, PCCP 7 (2005) 1100–1102.
[69] G.M. Pieper, C.C. Felix, B. Kalyanaraman, M. Turk, A.M. Roza, Detection by ESR of DMPO hydroxyl adduct formation from islets of langerhans, Free Radical Biol. Med. 19 (2) (1995) 219–225.
[70] J.-I. Ueda, K. Takeshita, S. Matsumoto, K. Yazaki, M. Kawaguchi, T. Ozawa, Singlet Oxygen–mediated Hydroxyl Radical Production in the Presence of Phenols: Whether DMPO–·OH Formation Really Indicates Production of ·OH? Photochem. Photobiol. 77 (2003) 165–170.
[71] S.K. Jackson, M.P. Thomas, S. Smith, M. Madhani, S.C. Rogers, P.E. James, In vivo EPR spectroscopy: biomedical and potential diagnostic applications, Faraday Discuss. 126 (2004) 103–117.
[72] L.u. Yang, A. Hakki, F. Wang, D.E. Macphee, Different Roles of Water in Photocatalytic DeNOx Mechanisms on TiO2: Basis for Engineering Nitrate Selectivity? ACS Appl. Mater. Interfaces 9 (20) (2017) 17034–17041.
[73] J. Zhang, X. Liu, X. Suo, P. Li, B. Liu, H. Shi, Facile synthesis of Ag/AgCl/TiO2 plasmonic photocatalyst with efficiently antibacterial activity, Mater. Lett. 198 (2017) 164–167.
[74] S. Min, F. Wang, G. Lu, Graphene-induced spatial charge separation for selective water splitting over TiO2 photocatalyst, Catal. Commun. 80 (2016) 28–32.